Proceedings of the European Conference Physics of Magnetism, Poznań 2017

Magnetisation and Hydrogenation of Mg/Ni Multilayers

S. Pacanowski[a,*], A. Marczyńska[a], H. Dawczak-Dębicki[a,c], B. Jabłoński[a,b], B. Szymański[a] and L. Smardz[a]

[a]Institute of Molecular Physics, Polish Academy of Sciences, M. Smoluchowskiego 17, 60-179 Poznań, Poland
[b]Faculty of Technical Physics, Poznań University of Technology, Piotrowo 3, 60-965 Poznań, Poland
[c]Faculty of Physics, Adam Mickiewicz University, Umultowska 85, 61-614 Poznań, Poland

In this contribution we have studied magnetisation of Mg/Ni multilayers (MLs) to characterise the alloing effect near interfaces. The layered structure was characterised by standard X-ray diffraction. The MLs were deposited by UHV magnetron sputtering onto naturally oxidised Si(100) substrates. Results showed, that due to Mg-Ni alloy formation near interfaces the magnetizations of the MLs were strongly reduced. Effective "dead" Ni layer thickness was estimated as 1.2 nm at room temperature (RT). Furthermore, hydrogen absorption kinetics at a pressure of about 1000 mbar was studied at RT in Pd covered Mg/Ni MLs using four-point resistivity measurements. Results showed that the fastest initial rise in resistance in the first 9 s was observed for $d_{\mathrm{Ni}} = 3.5$ nm.

DOI: 10.12693/APhysPolA.133.617
PACS/topics: 75.70.Cn, 61.10.Nz

1. Introduction

An optimal metal-hydride system has a hydrogen equilibrium pressure of 1 bar at room temperature. Because of weight constraints the interest of the scientific community has turned to lightweight hydride-forming elements such as Li, B, Na, Mg, and Al [1]. The strong interest in pure Mg and Mg-based alloys as hydrogen storage materials arises from the fact that Mg can absorb and desorb a large amount of hydrogen [1–2]. Moreover, magnesium is abundant, light weight, and can contain 7.6 wt.% of hydrogen. To improve the hydrogenation kinetics and thermodynamics extensive researched has been performed on the field of microstructure and catalysis [3–5]. Not only from a storage point of view are pure magnesium and magnesium-based alloys the subject of intensive studies, but also as thin film materials magnesium have very interesting properties [6–7]. Switchable mirrors based on magnesium alloys that can be reversibly switched between a mirror and low-impedance state and a transparent and high-impedance one have attracted great interests in exploring new photoelectric devices, such as H_2 sensor and smart windows [6–7]. However, the reversible optical and electrical transitions of Mg film are to slow due to the low hydrogen diffusion rate inside film. The retarded optical and electrical transitions in Mg film were also ascribed to the formation of a blocking MgH_2 layer at the interface between Pd and Mg under the H_2 pressure higher than 1 bar. This MgH_2 layer prevents hydrogen to diffuse into the underlying unreacted metallic Mg since the hydrogen diffusion rate in MgH_2 phase is three orders of magnitude lower than that in Mg phase [8].

Thermodynamic stability of the Mg-H system can be drastically modified via elastic constraints [9]. This is a direct consequence of the long-range H-H interaction in metals [10]. In a metal with elastically free surfaces two hydrogen atoms feel an effective attractive interaction, while in a sample clamped on all sides the interaction become repulsive. It was also shown a possibility to tailor the thermodynamics of a metal-hydrogen system by means of elastic constraints [9]. Thin films of Mg were used as a model metal-hydrogen system. Elements immiscible with Mg (for instance Ti) behave like scissors, while elements forming an alloy with Mg exert a clamping effect that leads to huge increases in hydrogen equilibrium pressures. Clamping arises as a consequence of alloying between Mg and the top layer (for instance Ni), and its effects can be understood on the basis of a simple elastic model [9].

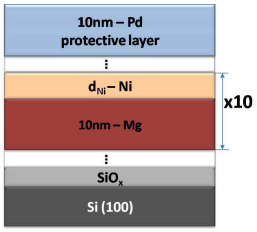

Fig. 1. Schematic description of prepared Mg/Ni MLs.

In this paper we study magnetisation of Mg/Ni multilayers (MLs) to characterise the alloying effect at the Mg-Ni and Ni-Mg interfaces. Moreover, hydrogen absorption kinetics at a pressure of about 1000 mbar was measured at room temperature (RT) in Pd covered Mg/Ni MLs.

2. Experimental procedure

Mg/Ni MLs were prepared at RT using UHV (5×10^{-10} mbar) magnetron sputtering [11–13]. In Fig. 1 we show a schematic description of prepared Mg/Ni MLs. As a substrate we have used Si(100) wafers with naturally oxidised surface to prevent a silicide formation. Therefore we have applied a special heat treatment in UHV before deposition in order to obtain a smooth SiO_x

*corresponding author; e-mail: sebastian@ifmpan.poznan.pl

surface layer. The Mg-layers with a constant thickness of $d_{\mathrm{Mg}} = 10$ nm were deposited using a radio frequency (RF) current source.

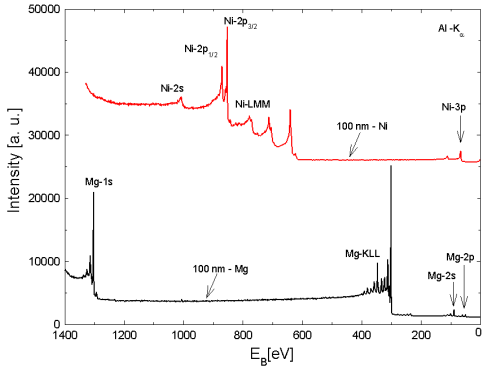

Fig. 2. XPS spectra (Al-K$_\alpha$) of *in-situ* prepared Ni and Mg thin films.

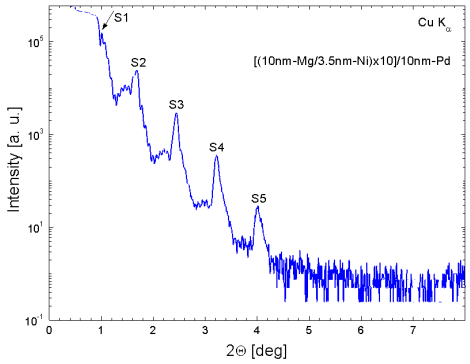

Fig. 3. Low-angle XRD (Cu-K$_\alpha$) pattern for Mg/Ni multilayer with Ni layer thickness of 3.5 nm.

For preparation of the Ni-layers ($0 < d_{\mathrm{Ni}} < 5$ nm) a direct current (DC) source was used. The deposition rates of Ni and Mg were individually checked by quartz thickness monitors. The thickness of individual layers were controlled by varying their deposition times. Furthermore, the calibrations of the deposition rates were also determined by thickness measurements of reference samples using DEC-TAC (Bruker) profilometer and X-ray fluorescence analysis. The number of repetition was equal to 10. Finally, a protective layer of 10 nm Pd was deposited to allow a fast uptake and release of hydrogen at RT and to avoid oxidation of the top Ni sublayer [14, 15].

The chemical composition of all the layers was checked *in-situ*, immediately after deposition, transferring the samples to an UHV (4×10^{-11} mbar) analysis chamber equipped with X-ray Photoelectron Spectroscopy (XPS). Details of the XPS measurements can be found in Ref. [16–18]. The XPS spectra were measured at RT using a SPECS EA 10 PLUS energy spectrometer with Al-K$_\alpha$ radiation of 1486.6 eV. The energy spectra of the electrons were analysed by a hemispherical analyser (FWHM$_{\mathrm{Mg-K}\alpha}$ = 0.8 eV for Ag-3$d_{5/2}$). All emission spectra were measured immediately after the sample transfer in vacuum of 8×10^{-11} mbar.

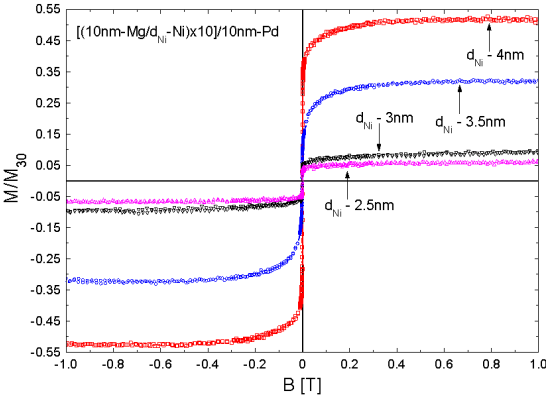

Fig. 4. Magnetic hysteresis loops of Mg/Ni MLs measured at RT for constant-thickness Mg (10 nm) and variable Ni layer thickness of 2.5, 3, 3.5, and 4 nm.

The structure of the Mg/Ni MLs was examined using standard $\theta - 2\theta$ X-ray diffraction (XRD). Hydrogen loading was performed in the HV chamber evacuated to about 10^{-6} mbar. Absorption kinetics at a pressure of about 1000 mbar was studied at RT in Pd covered Mg/Ni MLs using four-point resistivity measurements. Before hydrogenation the surfaces of the samples were outgassed at 450 K for 1h. The above procedure does not change the hysteresis loops of the "as prepared" samples. The magnetic characterisation of the MLs was carried out using a Vibrating Sample Magnetometer (VSM) at RT in an in-plane magnetic field up to 2 T.

3. Results and discussion

XPS core-level spectra for the freshly prepared 100 nm - Ni and 100 nm - Mg thin films are shown in Fig. 2. As can be observed, the oxygen and other impurities are absent on the surface of such prepared thin films. Practically no XPS signal from potential contamination atoms like O-1s and C-1s is was observed in Fig. 2.

Figure 3 shows low-angle XRD pattern for Mg/Ni MLs with Mg and Ni sublayer thicknesses of about 10 nm and 3.5 nm, respectively. The observed satellite reflections up to 5th order revealed good layered structure of the sample. The modulation wavelengths (Mg+Ni sublayer thickness) were calculated from the spacing between satellites peaks in the low-angle XRD for all of the prepared MLs. The results were consistent with the values obtained from total thickness divided by number of repetitions.

The in-plane hysteresis loops measured for Ni sublayer thickness varied from 2.5 to 4 nm are shown in Fig. 4. The magnetisations of the Mg/Ni MLs shown in Fig. 4 were normalised to the magnetisation of the 30 nm – Ni layer with the same sample area (15 mm x 15 mm). The magnetisation of the Mg/Ni MLs can be described by a

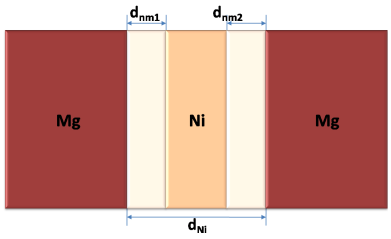

Fig. 5. Visualization of the non-magnetic alloy formation at the Mg-Ni and Ni-Mg interfaces.

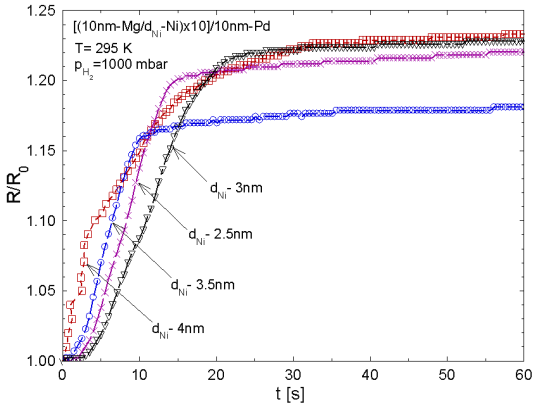

Fig. 6. Relative resistance as a function of hydrogenation time at a pressure of 1000 mbar measured at room temperature for Mg/Ni MLs covered by 10 nm of Pd protective layer.

simple model with a non-magnetic ("dead") layer at the Mg/Ni and Ni/Mg interfaces (see Fig. 5). For a simplicity we have assumed symmetric interfaces ($d_{\mathrm{nm1}} = d_{\mathrm{nm2}} = d_{\mathrm{nm}}$). The "dead layer" model was described in more details in Ref. [19]. In this model the Ni sublayer of thickness d_{Ni} is divided into a non-magnetic layer of thickness d_{nm} at each Mg interface and ferromagnetic layer of thickness (d_{Ni} - $2d_{\mathrm{nm}}$) at the centre of the Ni layer. The magnetisation of the Ni sublayers (M) relative to the magnetisation of pure 30 nm Ni film (M_{30}) can be written as follows [19]:

$$M/M_{30} = (d_{\mathrm{Ni}} - 2d_{\mathrm{nm}})/d_{\mathrm{Ni}}. \qquad (1)$$

To estimate the effective non-magnetic Ni layer thickness at the Mg-Ni and Ni-Mg interfaces (d_{nm}), we have used the Eq. (1) in the form: $(\mathrm{M}{\cdot}d_{\mathrm{Ni}})/\mathrm{M}_{30} = (d_{\mathrm{Ni}} \quad -2d_{\mathrm{nm}})$. From the linear regression fit we have estimated an effective non-magnetic Ni layer thickness at RT near the interfaces as $d_{\mathrm{nm}} \approx 1.2$ nm. The relatively high d_{nm} value revealed a significant alloying effect in the Mg/Ni MLs.

In Fig. 6 we show the resistance (R) of the hydrogenated Mg/Ni multilayer relative to the resistance of the "as prepared sample" (R_0) as a function of hydrogenation time at a pressure of 1000 mbar measured at RT. Results showed that the fastest initial rise in resistance in the first $\sim$ 9 s was observed for $d_{\mathrm{Ni}} = 3.5$ nm. However, the R/R_0 value increases slowly reaching the saturation ratio of $R/R_0 \approx 32$ after 3.5 h of hydrogenation for $d_{\mathrm{Ni}} = 3.5$ nm. For Ni sublayer thickness of 2.5, 3, and 4 nm the hydrogenation time needed to saturation is much longer.

In conclusions, due to Mg-Ni alloy formation near interfaces the magnetizations of the MLs were strongly reduced. Effective non-magnetic "dead" Ni layer thickness was estimated as 1.2 nm at room temperature. The hydrogen absorption kinetics depends on nickel sublayer thicknesses. The fastest initial rise in resistance in the first 9 s was observed for $d_{\mathrm{Ni}} = 3.5$ nm.

Acknowledgments

The first author (S.P.) would like to thank the Ministry of Science and Higher Education in Poland for financial support within the research project "Diamond grant", 2015-19, No. DI2014010344.

References

[1] L. Schlapbach, A. Züttel, *Nature* **414**, 353 (2001).

[2] Yahui Sun, Chaoqi Shen, Qiwen Lai, Wei Liu, Da-Wei Wang, Kondo-Francois Aguey-Zinsou, *Energy Storage Materials* (2017), in print.

[3] G. Barkhordarian, T. Klassen, R. Bormann, *J. Phys. Chem. B* **110**, 11020 (2006).

[4] G. Barkhordarian, T. Klassen, R. Bormann, *J. Alloys Compd.* **407**, 249 (2006).

[5] M. Dornheim, S. Doppiu, G. Barkhordarian, U. Boesenberg, T. Klassen, O. Gutfleisch, R. Bormann, *Scr. Mater.* **56**, 841 (2007).

[6] R. J. Westerwaal, C. P. Broedersz, R. Gremaud, M. Slaman, A Borgschulte, W. Lohstroh,K.G. Tschersich, H.P. Fleischhauer, B. Dam, R. Griessen, *Thin Sol. Films* **516**, 4351 (2008).

[7] Q. Zhao, Y. Li, Yun Song, X. Cui, D. Sun, F. Fang, *Appl. Phys. Lett.* **102**, 161901 (2013).

[8] A. Borgschulte, J. H. Rector, H. Schreuders, B. Dam, R. Griessen, *Appl. Phys. Lett.* **90**, 71912 (2007).

[9] A. Baldi, M. Gonzalez-Silveira, V. Palmisano, B. Dam, R. Griessen, *Phys. Rev. Lett.* **102**, 226102 (2009).

[10] H. Zabel, H. Peisl, *Phys. Rev. Lett.* **42**, 511 (1979).

[11] L. Smardz, K. Le Dang, H. Niedoba, K. Chrzumnicka, *J. Magn. Magn. Mater.* **140-144**, 569 (1995).

[12] L. Smardz, *Sol. State Com.* **112**, 693 (1999).

[13] L. Smardz, K. Smardz, H. Niedoba, *J. Magn. Magn. Mater.* **220**, 175 (2000).

[14] L. Smardz, U. Kobler, W. Zinn, *J. Appl. Phys.* **71**, 5199 (1992).

[15] J. Skoryna, S. Pacanowski, A. Marczyńska, M. Werwiński, Ł. Majchrzycki, R. Czajka, L. Smardz, *Surf. Coat. Techn.* **303**, 125 (2016).

[16] K. Smardz, L. Smardz, I. Okonska, M. Nowak, M. Jurczyk, *Int. J. Hydrog. Energy* **33**, 387 (2008).

[17] M. Jurczyk, L. Smardz, M. Makowiecka, E. Jankowska, K. Smardz, *J. Phys. Chem. Sol.* **65**, 545 (2004).

[18] J. Skoryna, A. Marczyńska, L. Smardz, *J. Alloys Comp.* **645**, S384 (2015).

[19] L. Smardz, *J. Alloys Comp.* **395**, 17 (2005).